SUPPLEMENTARY MATERIALS
to the article V.S. Ruzanova, S.G. Oshikhmina, G.S. Ritter, E.V. Dolgova, S.S. Kirikovich, E.V. Levites, Y.R. Efremov, T.V. Karamysheva, A.G. Bogomolov, M.I. Meschaninova, A.L. Mamaev, O.S. Taranov, S.V. Sidorov, S.D. Nikonov, O.Y. Leplina, A.A. Ostanin, E.R. Chernykh, N.A. Kolchanov, A.S. Proskurina, S.S. Bogachev "Concept of natural genome reconstruction. Part 3. Analysis of changes in the amount of telomeric DNA in colony cells as a new amplified feature that arose during the processing of hematopoietic bone marrow stem cells"

Supplementary Material 1. Brief information about factors involved in the processes described

ATM (ataxia telangiectasia mutated protein) – serine/threonine-specific protein kinase that is recruited and activated by double-strand DNA breaks; it phosphorylates several key proteins that initiate cell cycle arrest and induce DNA repair or apoptosis.

ATR (ATM and Rad3-related protein kinase) – serine/threonine-specific protein kinase that senses DNA breaks and, if any are detected, induces cell cycle arrest in the checkpoint; it is activated in the presence of single-stranded DNA.

ATRIP – the protein that recognizes single-stranded DNA coated with replication protein A; it works in a complex with ATR.

BFU-E (burst forming unit-erythroid) – an erythroid precursor.

BRCA1 (p220) (breast cancer 1) – the protein involved in the repair of DNA single-strand breaks at terminal R-loop domains.

BRCA2 (breast cancer 2) – the protein involved in chromosomal break repair and playing a crucial role in error-free repair of double-strand DNA breaks.

c-Abl (abelson murine leukemia viral homolog 1) – tyrosine kinase that is involved in cell cycle regulation and induces cell growth arrest and apoptosis under certain conditions.

CDC25 – phosphatase involved in regulation of the cell cycle.

CDC45, MCM2-7 – the components of the CMG complex (eukaryotic CMG helicase).

CDK (cyclin-dependent kinases) – the key enzymes involved in regulation of the eukaryotic cell cycle.

CFU-GM (colony-forming unit-granulocyte-macrophage) – a precursor for myeloid cells (myeloblasts).

Chk1, Chk2 (checkpoint kinase 1, 2) – checkpoint kinases involved in cell cycle arrest.

c-Kit, ScaI, CD34 – markers of poorly differentiated hematopoietic precursor cells.

CST – the single-stranded DNA-binding complex consisting of three proteins: CTC1, STN1, and TEN1; it is involved in regulation of telomere replication and chromosome end capping.

KAT5 – acetylase involved in ATM activation.

MRN complex – the complex consisting of the MRE11, RAD50, and NBS1 proteins; it recognizes double-strand breaks, prepares DNA ends for repair, activates ATM, and is involved in non-homologous DNA end joining and homologous recombination.

NHEJ (non-homologous end joining) – non-homologous repair of double-strand breaks.

p21 – the gene whose product regulates the G1/S transition.

p53 – the transcription factor regulating the cell cycle; a tumor suppressor.

POT1 – the protein recognizing the 3′ single strand and binding to the single-/double-stranded DNA, thus preventing telomeric instability.

RAD17, RAD9 – proteins playing a role in regulation of S phase in response to DNA damage.

RAD51 – the protein promoting strand exchange during homologous recombination and involved in D-loop formation.

Rb/E2F – the complex involved in the mechanism of G1-phase cell cycle arrest.

TERC (telomerase RNA) – telomerase RNA component.

TERT – telomerase reverse transcriptase.

TOPBPI – the protein directly stimulating the kinase activity of the ATR-ATRIP complex.

Topo II – topoisomerase II immobilizing the base of transcription loops.

TPP1 – the POT1- and TIN2-interacting protein, which recruits telomerase to telomeres and directly contacts telomerase.

TRF1 (telomeric repeat-binding factor 1) – recognizes the TTAGGG sequences.

TRF2 (telomeric repeat-binding factor 2) – promotes t-loop formation.

DNA-PK (DNA-dependent protein kinase) – protein kinase involved in the repair of double-strand DNA breaks.

Shelterin – the protein complex protecting and regulating telomeres; it consists of six proteins: TPP1, POT1, TRF1, TRF2, TIN2, and RAP1.

Supplementary Material 2. Analysis of the cellular response to perturbations of the higher-order chromatin structure

In the cell, there are several general cellular factors that are responsible for the occurrence of DNA damage, such as double-strand breaks or single-stranded DNA, and send signals about it to the cell. Activation of hierarchical kinases ATM, ATR, and DNA-PK, which belong to the family of phosphatidylinositol 3-kinase-related kinases, induces a cascade of events involving cellular response to double-strand breaks, replication fork stalling, or general perturbation of the higher-order chromatin structure (i. e., to stresses associated with gross chromatin structure disruption requiring mandatory attention from the cell and repair). The three types of signal transduction kinases ATM, ATR, and DNA-PK are interchangeable but exhibit greater specificity for different types of damage.

ATM is the first kinase to be activated in response to the emergent DNA double-strand breaks; it subsequently phosphorylates its kinase substrate, including DNA-PK, which is involved in double-strand break repair, as well as the factors responsible for cell cycle arrest (Chk1, Chk2, and p53).

Induction of cell cycle arrest is driven by phosphorylation of Chk1 and Chk2, which in turn hyperphosphorylate CDC25 phosphatase, thus inactivating it. Normally, CDC25 dephosphorylates the cyclin/cyclin-dependent protein kinase complex (CDK) and maintains its working state. Hyperphosphorylation of CDK is associated with inhibition of CDC45 transfer to the DNA replication origin (Sørensen et al., 2003). Hence, CDC25 regulates cell cycle progression through activation of CDK, which, along with activating the Rb/E2F pathway, is involved in activation of MCM2-7 hexamer (DNA helicase), a component of the pre-replication complex catalyzing melting of DNA strands during replication.

The p53-metabolic pathway of cell cycle arrest is associated with transcription of the *p21* gene, which is initiated by activated tumor suppressor gene; its protein product binds and inhibits cyclin–CDK complexes. As a result, unphosphorylated Rb retains E2F, and the cell division cycle is stopped (Bakkenist, Kastan, 2015).

Hence, ATM activation followed by the phosphorylation cascade, eventually leading to cell cycle arrest, is a response to double-strand breaks in DNA.

The least understood stage is at what time point the repair process leading to ATM activation is initiated. Literature analysis revealed that ATM can be simultaneously activated by several initiating vectors of different functional systems of the cell. However, perturbations of the higher order chromatin structure are believed to be the key initiating factor. Those are either double-strand breaks or chromatin decondensation caused by any of the factors reported in the literature. Disruption of the higher order (condensed) chromatin structure results in ATM activation. ATM can be autophosphorylated, or acetylated by KAT5 followed by autophosphorylation. ATM can be phosphorylated by ATR upon primary ATR activation as a result of replication fork stalling and formation of single-stranded DNA regions.

An analysis of the ATM phosphorylation kinetics indicates that ATM can be activated by perturbations of the higher-order chromatin structure. Exposure of cells to various non-DNA damaging agents, such as hypotonic stress, chloroquine, histone deacetylase inhibitor trichostatin A, insulin shock, mitochondrial electron transfer chain inhibitor, and other metabolic stresses, leads to chromatin perturbation without formation of double-strand breaks (Olcina et al., 2014). ATM is phosphorylated at serine 1981, which is accompanied by kinase activation. H2AX phosphorylation is not detected for these treatments. Furthermore, the MRN complex does not need to be present for ATM activation in this case. Immunostaining of phosphorylated protein indicates that ATM is diffusely distributed in the nuclear space. It is suggested that chromatin decondensation is permissive for KAT5 binding to H3K9me3 and H3K36me3, c-Abl dependent Tyr44 phosphorylation of KAT5, followed by a cascade of activating events (Bakkenist, Kastan, 2015).

KAT5 is one of the known agents initiating double-strand break repair. The emergence of DNA breaks is known to be followed by KAT5-dependent acetylation of ATM. Immediately after a break takes place, perturbation and loosening of chromatin as well as displacement of histones occur at the site of DNA damage. Altered chromatin compaction allows KAT5 to bind to H3K9me3 and/or H3K36me3 histones, which function as allosteric inducers activating KAT5 acetylation of ATM at lysine 3016. Binding of KAT5 to H3K9me3

occurs in a complex with ATM. This event leads to Tyr44 phosphorylation of KAT5 by c-Abl tyrosine kinase and activation of its acetylation domain. KAT5 acetylates ATM. The inactive enzyme dimer decomposes into monomers, and ATM is autophosphorylated. Next, ATM activated in response to DNA damage (double-strand breaks) activates Chk1, Chk2, and p53, leading to cell cycle arrest mediated by the aforedescribed cascade phosphorylation of different effector molecules. The c-Abl tyrosine kinase is a ubiquitously expressed kinase that is present in both the cytoplasm and the nucleus. The physical interaction between the KAT5–ATM complex and H3K9me3 apparently initiates recruitment to the binding site of c-Abl tyrosine kinase, which is ubiquitously expressed in the nuclear space, leading to phosphorylation and activation of acetylase. The association of KAT5 with H3K9me3 residing in inactivated chromatin and with H3K36me3 residing in active chromatin, as well as chromatin decondensation in the domain flanking double-strand breaks are the central molecular mechanisms of ATM activation (Meltser et al., 2011; Bakkenist, Kastan, 2015; Mahajan K., Mahajan N.P., 2015).

An important aspect of ATM activation is its molecular interplay with another hierarchical kinase, ATR. The ATM-related protein kinase ATR is activated in response to emergence of single-strand DNA regions as a result of formation of double-strand breaks, replication fork stalling, and other perturbations of the chromatin structure causing the emergence of unpaired DNA regions. When single-strand DNA regions occur, they are immediately coated by replication factor A. The involvement of several cofactors (RAD17-RFC2-5, RAD9-RAD1-HUS1 (9-1-1), ATR-ATRIP, and TOPBP1) causes ATR activation and repair response. ATM and ATR exhibit different substrate specificities and can interact with each other. Both kinases affect each other's recruitment to the damage site. ATM provides conditions for ATR activation by processing double-strand ends. On the other hand, ATR can phosphorylate H2AX in response to replication fork stalling, thus recruiting ATM to the stall site. Both kinases can also directly phosphorylate each other in response to replication stress. Both ATM and ATR can affect the localization and function of their regulators. This interplay between the two hierarchical kinases suggests that any alteration in the higher-order chromatin structure and the emergence of specific intermediates that necessarily activate one of the kinases will induce the cell cycle arrest and mechanisms of repair of the perturbated higher-order chromatin structure (Maréchal, Zou, 2013).

Supplementary Material 3. Choosing the approach to properly measure the telomeric DNA content in the cells treated with inducers, hDNA^{gr} and angiogenin, in the mouse model

A series of analytical experiments using a mouse model were conducted. Three principal methodological approaches for quantifying the telomeric DNA content were elaborated. It was supposed that the results obtained would be used to choose an adequate, unambiguously interpretable methodology for measuring the telomeric DNA content in rats and for the model of cryopreserved human bone marrow.

Mouse bone marrow cells were treated with hDNA^{gr} and angiogenin inducers and inoculated onto methylcellulose. The cells were harvested after 9 days. DNA was isolated from a portion of the cells; real-time PCR and dot blot hybridization were performed. Another portion of the cells from the same sample was treated with colchicine, and FISH was carried out.

Real-time PCR

A method for measuring the telomeric DNA content by real-time PCR has been reported in the literature. The approach was demonstrated for a mouse model and is believed to be reliable (Cawthon, 2002; Stefler et al., 2018). We have fully reproduced the real-time PCR technique to measure the telomeric DNA content in the selected mouse model system. Real-time PCR was conducted on a QuantStudio 5 real-time PCR system (Applied Biosystems, USA) with primers specific to telomere repeat sequences and the single-copy *36B4* gene to quantify the telomeric DNA content (Table 1).

Table 1. Sequences of the primers used

Name	Structure
Tel-for	5′ CGG TTT GTT TGG GTT TGG GTT TGG GTT TGG GTT TGG GTT 3′
Tel-rev	5′ GGC TTG CCT TAC CCT TAC CCT TAC CCT TAC CCT TAC CCT 3′
36B4-for	5′ ACT GGT CTA GGA CCC GAG AAG 3′
36B4-rev	5′TCA ATG GTG CCT CTG GAG ATT 3′

PCR was conducted using primers specific to telomere repeat sequences (Fig. 1*A*) and the single-copy *36B4* gene (Fig. 1*B*). In several experimental replicates, 100–500 bp DNA fragments were used. The findings obtained using this DNA were opposite to the expected ones. In the case of using the hDNA^{gr} activator, the telomeric DNA content detected by this approach was significantly lower than that in the control sample (Fig. 1*C*). A rather adequate result was obtained when the hydrolyzed template was replaced with a non-sonicated one (Fig. 1*D*).

Nevertheless, the content of detectable telomeric DNA in the samples "with an inducer" was not significantly higher than that in the control samples. We attribute the revealed discrepancy from the expected result to the following fact. Telomeric DNA fragments hydrolyzed by sonication to "the size of a primer" (100–500 bp) per se are quasi-primers and anneal to each other, thus occupying the landing sites for working primers. The higher the content of competitive telomeric DNA, the more telomeric fragments anneal to their own sequence (the absence of the 3′ end needed for polymerase binding, caused by annealing yielding 3′ blunt ends and overhangs or by nonspecific breakage of the phosphodiester bond), and the lower are the chances for the working primer to find the template and yield the PCR product. In other words, as suggested previously, the obtained result mirrored the actual situation with the expected increase in telomere length (the rise in telomeric DNA content).

When angiogenin was used as an inducer, the telomeric DNA content statistically significantly increased in the experiment with nonsonicated genomic DNA (Fig. 1*D*).

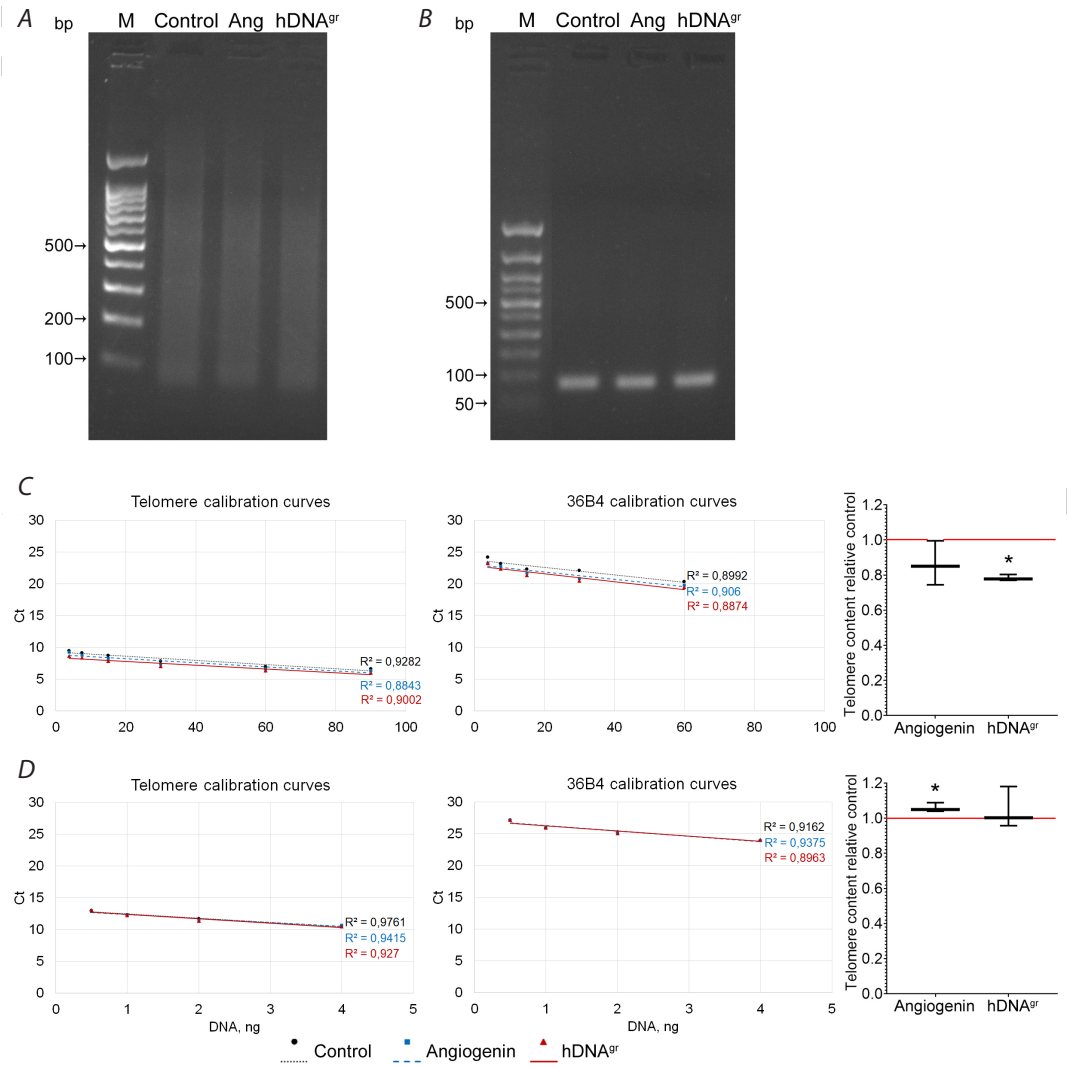

Fig. 1. *A* – electrophoresis of PCR products with primers specific to telomere repeat sequences; *B* – electrophoresis of PCR products with primers specific to the *36B4* gene; *C*, *D* – results of real-time PCR with a sonicated (*C*) and nonsonicated (*D*) template. The calibration curves with primers specific for telomere repeat sequences and the *36B4* gene and the diagram showing the telomeric repeat content relative to the control group where the telomeric repeat content is taken as unity (the red line). * Differences are statistically significant compared to the control group; $p < 0.05$, Mann–Whitney U-test.

FISH

In situ hybridization was carried out using the same cellular material.

FISH was performed according to the standard procedure using telomeric hexanucleotide $(CCCTAA)_3$ as a probe (the TelPNA-Cy3 probe). Fluorescence signals were detected using an Axioskop 2 Plus fluorescence microscope (Zeiss) and the ZEN software.

In order to prepare metaphase chromosome specimens, cultured cells were incubated in a growth medium supplemented with 0.1 μg/mL colcemid (Biological Industries) for 2 h. Cells were pelleted by centrifuging (200g, 5 min) and treated with a hypotonic solution of 0.075 M KCl (Sigma-Aldrich, USA) for 20 min at 37 °C. The cells were then re-pelleted by centrifuging and fixed with a fixative (3 : 1 methanol : acetic acid) replaced three times at –20 °C. The fixed cell suspension was stored in the fixative at –20 °C. Metaphase chromosome specimens were obtained by pipette dropping the cell suspension onto cold microscope slides from a height of 40 cm according to the procedure described in ref. (Henegariu et al., 2001). The specimens were stored at –20 °C.

In situ hybridization of the cloned sequences was conducted without suppression of repetitive sequences (Pinkel et al., 1988; Lichter et al., 1988). Briefly, cytology specimens of metaphase chromosomes were treated

with a pepsin solution in 10 mM HCl for 20 min at 37 °C, rinsed with phosphate-buffered saline (0.13 M NaCl; 0.27 mM KCl; 7 mM Na_2HPO_4; 3 mM NaH_2PO_4) at pH 7.4, and rinsed with phosphate-buffered saline supplemented with 50 mM $MgCl_2$ once. The cytology material was fixed in 1 % formaldehyde in phosphate-buffered saline supplemented with 50 mM $MgCl_2$ for 10 min at room temperature. After fixation, the specimens were washed in phosphate-buffered saline and then in phosphate-buffered saline supplemented with 50 mM $MgCl_2$, followed by dehydration in a series of increasing ethanol concentrations using the standard procedure.

DNA probe (200 ng/μL, 15 μl) pre-dissolved in hybridization buffer and labeled with TAMRA-dUTP (5-tetramethylrhodamine-dUTP, Roche, Switzerland) was carefully applied to the chromosomes spread on the microscope slide under a coverslip. The DNA probe and the template were co-denatured on a ThermoBrite instrument (StatSpin, USA) at 75 °C for 5 min. After denaturation, the specimens were quickly transferred to a humidity chamber and left overnight in a laboratory incubator (Incucell 55, BMT, Czech Republic) at 42 °C. Once the hybridization had been completed, the specimens were washed off the coverslips with 2×SSC (saline sodium citrate buffer). The excess unbound DNA probe was washed with 1×SSC for 5 min at 60 °C. The specimens were then transferred into 4×SSC/0.1 % NP-40 and incubated at 42 °C for 10 min on a rocking shaker. Next, the specimens were incubated in phosphate-buffered saline for 5 min at room temperature. Once incubation in PBS had been completed, the specimens were transferred to a beaker with distilled water, quickly dipped there, and transferred to a beaker with 70 % ethanol. The specimens were dehydrated in a series of increasing ethanol concentrations (70, 80, and 96 %), for 3 min at each concentration, at room temperature, followed by drying. After *in situ* hybridization, chromosomes were stained with DAPI (4,6-diamidino-2-phenylindole) fluorescent stain dissolved in an anti-fade medium (Vectashield antifade, 200 ng/mL, Vector Laboratories INC., USA).

Microscopic images in three cell specimens were recorded using Q-FISH with the TelPNA-Cy3 probe (Table 2).

The presence of TelPNA-Cy3 signal on metaphase plates and separately located interphase nuclei was analyzed. The IFI (integrated fluorescence intensity) values were determined. FISH signal of TelPNA-Cy3 was observed in all the centromeric and telomeric regions of acrocentric chromosomes. An additional signal on the long arm of one of the chromosomes was observed at the interstitial sites of the long arm of one of the chromosomes or homologs in all three cell specimens (Fig. 2*A*). In the control line, the number of interstitial signals was the lowest (4.5 %) (Table 2). They were detected on five chromosomes from three metaphase plates (in four cases, on individual arms of individual chromosomes, and in one case, on sister chromatids in the pericentromeric region of one of the chromosomes) (Fig. 2*A*). In the angiogenin-treated cell culture specimen, telomeric repeats at the interstitial sites of chromosomes were detected in 10 % of the metaphase plates analyzed (Table 2, Fig. 2*A*). Microscopic analysis of a $hDNA^{gr}$-treated cell culture specimen revealed interstitial segments in 7 % of metaphase plates (Table 2). Interstitial signals were observed on separate arms of individual chromosomes (Fig. 2*A*).

Images of metaphase plates with an identical number of chromosomes corresponding to the standard karyotype of the mouse, which consists of 40 acrocentric chromosomes, were selected to perform bioinformatics

Table 2. The number of metaphase plates and interphase nuclei analyzed in three cell lines

Параметр	Control	Angiogenin	$hDNA^{gr}$
Total analyzed	133	110	213
Number of interphase nuclei	45	33	73
Number of metaphase plates	77	62	121
Number of metaphase plates adjacent to the nucleus	11	15	19
Total metaphase plates	88	77	140
TelPNA-Cy3 signaling at metaphase plates	4	8	10

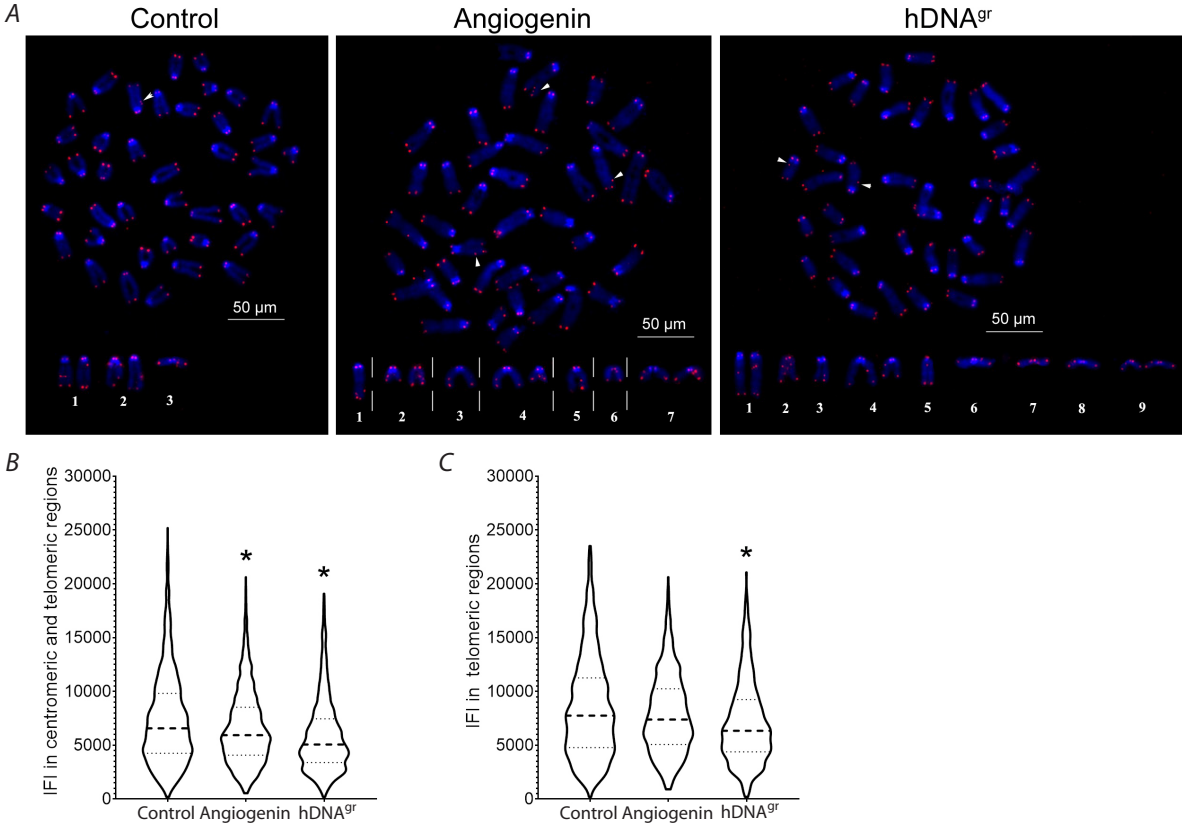

Fig. 2. The results of Q-FISH with TelPNA-Cy3 of three cell specimens: the control sample and the specimens treated with angiogenin and hDNA^{gr}.

A – metaphase plates with interstitial signals (shown with an arrow) are presented. Chromosomes containing interstitial segments are shown at the bottom; numbers correspond to the numbers of metaphase plates. Overall chromosome staining with DAPI (blue) and TelPNA-Cy3 staining (red); *B*, *C* – the IFI values in the centromeric and telomeric regions (*B*) or in the telomeric regions only (*C*) of metaphase chromosomes in three cell specimens. An aggregate of individual values (violin plots) is provided; the bold dotted line denotes the median values; the thin dotted line denotes the interquartile range. * Differences are statistically significant compared to the control group; $p < 0.0001$, Mann–Whitney U-test.

analysis of signal intensity (Fig. 2*B*, *C*) recorded by Q-FISH with the TelPNA-Cy3 probe and located in the centromeric and telomeric regions of chromosomes. As expected, fluorescence intensity would directly indicate the telomeric DNA content. It turned out that the fluorescence intensity was higher in the control than in the case of hDNA^{gr} and angiogenin inducers (Fig. 2*B*, *C*).

In order to assess the validity of the Q-FISH results, we compared the relative telomere lengths in sister chromatids. In most sister chromatids, the telomere lengths and the IFI values are expected to be identical. We observed a strong positive correlation for the IFI values of telomeres of sister chromatids (Spearman's rank correlation coefficient = 0.93–0.96). These data are indicative of proportional binding of DNA probes to telomeric repeats.

Hence, the results of bioinformatics analysis of signal intensity, once again, did not agree with the expected one (an increase in the telomeric DNA content).

First, this result can be possibly attributed to the hybridization procedure, analysis technique, and biological properties of telomeric heterochromatin. It is fair to assume that the telomeric DNA content increased significantly, resulting in supercompaction of telomeric regions. The hybridization procedure involves simple trypsin treatment and exposure to hypotonic stress without unwinding of the compacted chromatin loci. The accessible DNA regions get hybridized. Under these conditions, the probe will be hybridized with a smaller quantity of surface telomeric DNA because most DNA will exist in the telomere in a supercoiled form, thus being inaccessible to the probe.

The following fact can be the second explanation for the result. By day 9 of culturing on methylcellulose, cells in which pangenomic single-strand DNA breaks had been induced were not released from the cell cycle arrest associated with functional rearrangement of the cell mode (no one had a notion about it at the time when the experiment was conducted), while the telomeric DNA content had already been changed. The analyzed metaphase plates are a cell cycle phase of hematopoietic stem cells (HSCs), which were incapable of internalizing extracellular DNA fragments (e. g., were going through the G2/M phase when being treated with $hDNA^{gr}$ inducer (Dolgova et al., 2016)). In other words, cells, the precursors of which had not internalized extracellular fragments, were analyzed, and the result obtained refers to the cells not exposed to the analyzed effect.

The facts taken together demonstrated that the aforementioned methods for analyzing telomere length under the selected experimental conditions would yield results that can always be interpreted in different mechanistic ways. Therefore, we chose the method for measuring the telomeric DNA content using quantitative dot blot hybridization. This approach allowed us to directly estimate the content of DNA homologous to the probe used in the experimental sample regardless of the circumstances listed above.

Assessment of changes in telomeric DNA content by quantitative dot blot hybridization

Dot blot hybridization was carried out at the final stage of the analysis. DNA of the specimens was sonicated until fragments sized 100–500 bp were obtained. This was due to the fact that hybridization of nonsonicated DNA yielded conglomerates, which significantly complicated analyzing hybridization signals. It turned out that the telomeric DNA content in the specimens of DNA isolated from HSCs treated with $hDNA^{gr}$ within bone marrow cells is significantly and reliably higher than that in the control samples (C-probe) (in the article, Fig. 2*A*3). That is, dot blot hybridization is the only adequate method for quantifying telomeric DNA in our experiments.

Supplementary Material 4. Analysis of the correlation between the colony type and hybridization signal intensity

A correlation between the colony type and hybridization signal intensity was analyzed (Fig. 1).

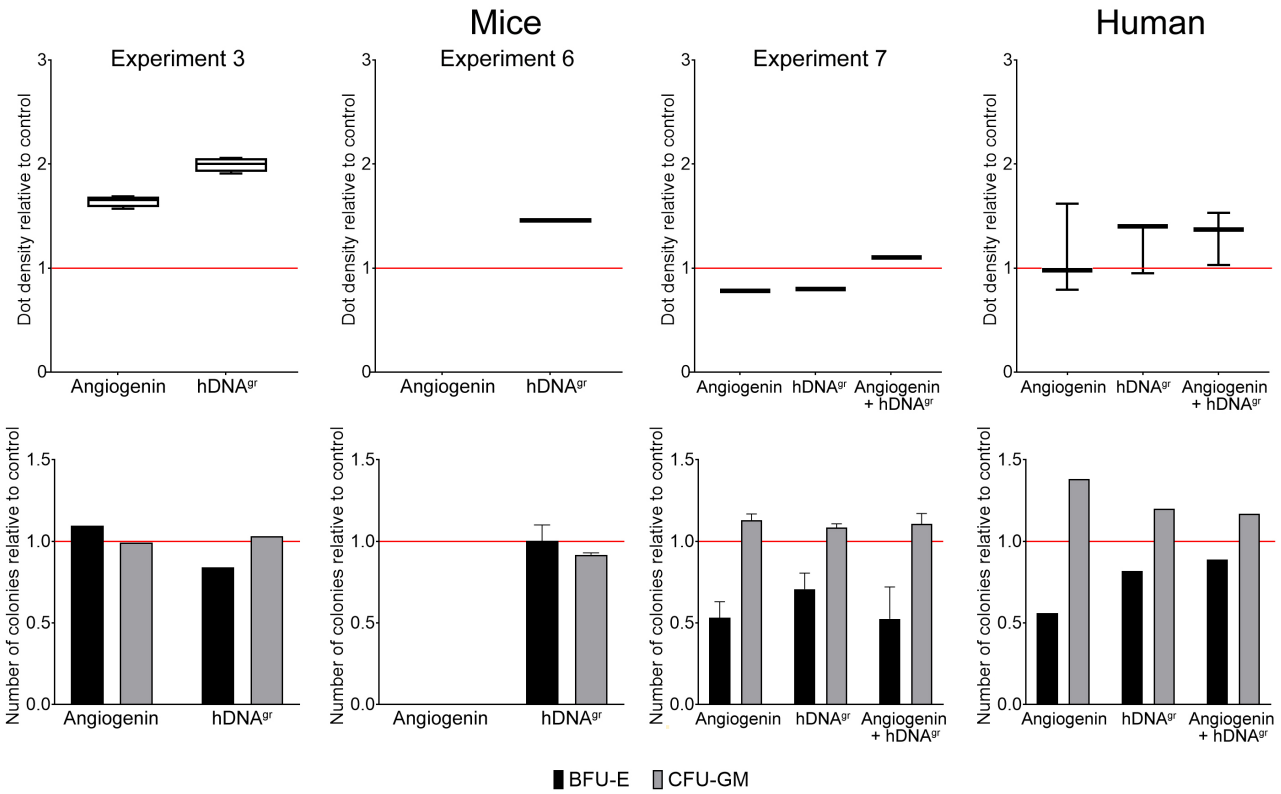

Fig. 1. Analysis of correlation between the hybridization signal intensity and the number and type of colonies in different experiments using mouse and human cells after treatment with angiogenin, hDNA^{gr}, and angiogenin + hDNA^{gr}.

Experiment 3, mice. In the hDNA^{gr} sample, the number of BFU-E colonies is smaller than that in the control, while the number of CFU-GM colonies is virtually the same as that in the control. Meanwhile, hybridization signal intensity is maximal. In the angiogenin sample, the number of BFU-E colonies is ~10 % larger than that in the control. The number of CFU-GM colonies is approximately the same as that in the control. Hybridization signal intensity is higher compared to that in the control but lower than that in hDNAgr. It can be inferred that in this experiment, for angiogenin, the telomeric DNA content can increase due to induction of activity of BFU-E colonies in the G0 phase, previously inactive in the bone marrow and having the telomeric DNA content predetermined at the embryonic stage. In the case of hDNA^{gr}, the rise in the telomeric DNA content is most likely not to be associated with the increased content of homotypic CFU-GM colonies. There is a minimal excess of the number of GM colonies. This increase can be related to 1) activity of the endo- or exo- telomerase gene; 2) direct integration of telomeric repeats into the HSC genome during treatment of bone marrow cells with hDNA^{gr} inducer; 3) or telomeric repeat amplification as a result of replication of a quasi t-loop formed by telomeric repeats of extracellular DNA; 4) preservation of telomeric DNA fragments initially internalized by HSCs in the cell in the non-integrated state throughout the entire period of cultivation on methyl cellulose; 5) mixed variants are possible.

Experiment 6, mice. An analysis was conducted for the correlation between hybridization signal intensity of DNA isolated from colonies produced from HSCs within bone marrow treated with two doses of hDNA^{gr} (50 and 500 μg per sample) and the type of colonies from which DNA was isolated for hybridization. It was shown in a particular experiment that hybridization signal intensity did not correlate with the colony type. The

hDNA^{gr} values at a dose of 500 μg per sample are plotted in the figure for hybridization signal intensity. The revealed differences can be indicative of one of the following: activation of both telomerase variants or integration of extracellular telomeric DNA into the HSC genome when processing bone marrow cells, or telomeric repeat amplification as a result of replication of the t-loop formed by telomeric repeats of extracellular DNA, or preservation of telomeric DNA fragments initially delivered to HSCs in the cell in a non-integrated state throughout the entire period of cultivation on methyl cellulose.

Experiment 7, mice. In the angiogenin+hDNA^{gr} sample, the number of BFU-E colonies was smaller than that in the control. The number of CFU-GM colonies was slightly (~10 %) larger compared to the control. The hybridization signal intensity for angiogenin and hDNA^{gr} was lower than that in the control. The hybridization signal intensity for a combination of inducers was slightly higher compared to the control.

Comparison of the data of experiments 3 and 7 for angiogenin suggests that the increase in telomeric DNA content can be attributed to induction of activity of BFU-E colonies in the G0 phase, which had previously been inactive in the bone marrow and had the telomeric DNA content predetermined at the embryonic stage. According to the findings of three experiments, for hDNA^{gr}, no correlation was revealed between hybridization signal intensity and prevalence of a certain colony type.

Experiments using the model of cryopreserved human bone marrow cells. For the angiogenin-treated sample, there was no significant difference in hybridization signal intensity compared to control DNA. The number of CFU-GM colonies was significantly larger compared to the control values. The number of BFU-E colonies was significantly smaller compared to the control. This pattern correlates with the data obtained for the mouse model.

For the hDNA^{gr} and angiogenin+hDNA^{gr} samples, hybridization signal intensity was significantly higher than that in the control. For this model system, the increase in the telomeric DNA content can possibly be associated with induction of activity of GM colonies in the G0 phase, which had previously been inactive in the bone marrow and had the telomeric DNA content predetermined at the embryonic stage. However, comparison of all the data obtained for both model systems revealed no correlation between hybridization signal intensity and prevalence of a certain colony type.

Supplementary Material 5. Assessment of the probability that residual hDNA^{gr} material can remain in HSCs after treating HSCs within the bone marrow with this DNA, which may cause an artifact of increased telomeric DNA content

First, the potential quantity of residual DNA was calculated. The idea of the experiment was to show that the quantity of extracellular dsDNA initially present in HSCs within the bone marrow is negligible by day 15 of colony growth and undetectable using the available experimental procedures. Initially, the quantity of residual DNA in colony-forming cells on day 15 was estimated.

The length of a single human telomere is ~10 kbp. The total length of telomeric DNA for all the chromosomes will be ~1,000 kbp (10^6 bp or 0.001 % of the haploid genome). HSCs within human bone marrow cells internalize 0.02 % of the haploid genome of extracellular dsDNA, which will contain 0.00002 % of telomeric DNA or 20,000 bp or 100–10 DNA fragments of specified size (200–2,000 bp) under normal fragment distribution. These fragments will be partitioned either equally or stochastically among daughter cells. Colonies containing up to ~1,000 cells will have been formed by day 15. That is, 10–100 DNA fragments of specified length (2,000–200 bp) are supposed to be distributed among ~1,000 progeny cells, corresponding to ~0.2–2.0 bp of telomeric repeat sequences per cell. At the known total length of human telomeres (~1,000,000 bp), the added specified quantity of telomeric DNA will lie within or lower than the noise level. The 20–100 % increase in telomeric DNA content obtained in the experiments compared to the control entirely rules out the probability that the results can be affected by the amount of residual telomeric DNA.

The following series of experiments were conducted in order to experimentally verify the calculations performed. Bone marrow cells harvested from Hodgkin lymphoma patients were incubated in the presence of PCR fragment, DNA of synthetic human *AluI* repeat flanked by pBS plasmid sequences with M13 primer landing sites (pBSM13-*AluI*-pBSM13), for 1 h in an atmosphere of 5 % CO_2 at 95 % humidity and 37 °C (1 μg per 10^6 cells in 1 mL of serum-free IMDM medium). At the aforementioned ratio and exposure time, the cells were fully saturated with extracellular dsDNA fragments (0.02 % in this study). After incubation, bone marrow cells were cultured in methylcellulose medium. On day 15 of cultivation, colony-forming cells were washed to remove the methylcellulose medium, and DNA was isolated from the cells. Human placental DNA was used as a negative control. Quantitative analysis of DNA molecules by real-time PCR was conducted using a BioMaster RT-qPCR kit (SYBR Green stain) (Biolabmix, Russia) on a QuantStudio 5 Real-Time PCR System. Standard M13 primer sequences and *AluI* repeat DNA as a template (0; 0.005; 0.05; 0.5; 5; 50 and 500 pg per reaction) were used to plot the qPCR calibration curve. The experiment was performed in three replicates for each sample concentration. The linear dependence between Ct and the content of *AluI* repeat DNA was plotted using Microsoft Excel. A total of 10 and 100 ng of DNA from colony-forming cells incubated with exogenous fragments of *AluI* repeat DNA and human placental DNA were employed for qPCR. The amount of the *AluI* repeat in the sample was estimated using Microsoft Excel. The resulting PCR products were detected by agarose gel electrophoresis.

Reactions were conducted for two DNA samples isolated from the cells of colonies produced by HSCs, subjected to primary treatment within bone marrow cells with human *AluI* repeat DNA flanked by sequences of pBS plasmid with M13 primer landing sites and human placental DNA. This approach was chosen in order to fully rule out the risk of contamination during the colony-stimulation experiment (DNA isolation from placenta was performed by a different laboratory employee at a different place). The quantity of DNA in the final cell supernatant before lysis was determined simultaneously.

It was found that the amount of residual DNA in the supernatant of pelleted cells before they were lysed for DNA extraction had been either below or at the sensitivity threshold of the lower standard of the highly sensitive DNA detection kit (Qubit). In other words, there was no internalizable substrate. Real-time PCR performed subsequently fully confirmed the calculations performed. By day 15 of cultivation on methylcellulose, the cells contained no detectable amount of the original *AluI* repeat DNA flanked by pBS sequences with M13 primers (Fig. 1). That is, the *AluI* repeat DNA molecules that had originally been internalized into HSCs treated with

this DNA within bone marrow cells were not detected in colony-forming cells. It means that the increase in the content of telomeric DNA detected in dot blot hybridization experiments cannot be caused by presence of residual original DNA in colony-forming cells. Furthermore, it follows that the *AluI* fragments, together with the non-homologous ends of pBSM13, are not incorporated into the genome that will be amplified.

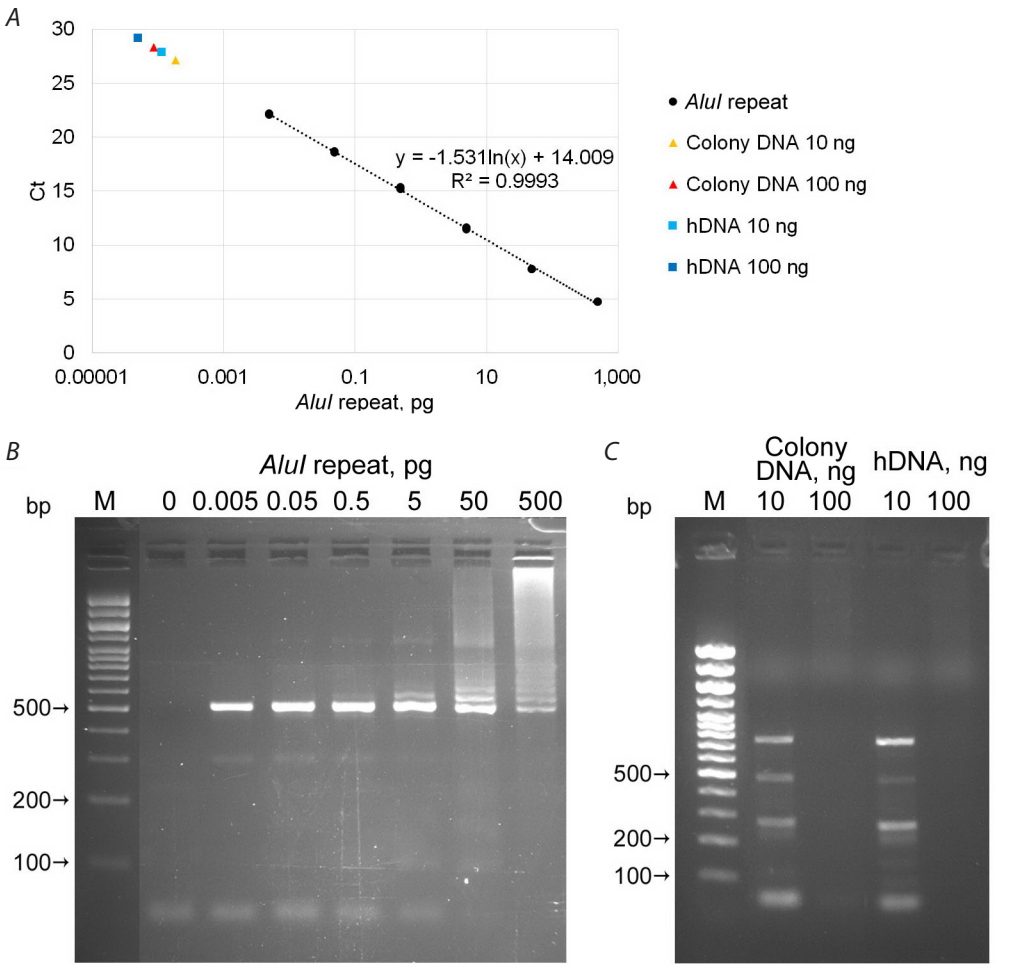

Fig. 1. An analysis of the probability of contamination (residual quantity of $hDNA^{gr}$ remaining in colony-forming cells after the initial internalization of extracellular fragments into HSCs within bone marrow cells). Evaluation of the possibility of integrating the pBSM13-AluI-pBSM13 PCR fragment into the genome of HSCs within bone marrow cells. The calibration curve (*A*) and gel electrophoresis (*B*, *C*) of the samples used for plotting the calibration curve, the pBSM13-*AluI*-pBSM13 PCR fragment consisting of a human *AluI* repeat flanked by plasmid sequences between the M13F/R primers. On the calibration curve, colored symbols denote the amount of target product in the samples of DNA isolated from colonies produced from the sample derived from bone marrow cells initially treated with pBSM13-*AluI*-pBSM13 substrate and from human placental DNA. Numbers denote the amounts of PCR template DNA.

References

Bakkenist C.J., Kastan M.B. Chromatin perturbations during the DNA damage response in higher eukaryotes. *DNA Rep*. 2015;36:8-12. doi 10.1016/j.dnarep.2015.09.002

Cawthon R.M. Telomere measurement by quantitative PCR. *Nucleic Acids Res*. 2002;30:e47. doi 10.1093/nar/30.10.e47

Dolgova E.V., Potter E.A., Proskurina A.S., Minkevich A.M., Chernych E.R., Ostanin A.A., Efremov Y.R., Bayborodin S.I., Nikolin V.P., Popova N.A., Kolchanov N.A., Bogachev S.S. Properties of internalization factors contributing to the uptake of extracellular DNA into tumor-initiating stem cells of mouse Krebs-2 cell line. *Stem Cell Res Ther*. 2016;7(1):76. doi 10.1186/s13287-016-0338-8

Henegariu O., Heerema N.A., Lowe Wright L., Bray-Ward P., Ward D.C., Vance G.H. Improvements in cytogenetic slide preparation: controlled chromosome spreading, chemical aging and gradual denaturing. *Cytometry*. 2001;43(2):101-109. doi 10.1002/1097-0320(20010201)43:2<101::AID-CYTO1024>3.0.CO;2-8

Lichter P., Cremer T., Borden J., Manuelidis L., Ward D.C. Delineation of individual human chromosomes in metaphase and interphase cells by in situ suppression hybridization using recombinant DNA libraries. *Hum Genet*. 1988;80(3):224-234. doi 10.1007/BF01790090

Mahajan K., Mahajan N.P. Cross talk of tyrosine kinases with the DNA damage signaling pathways. *Nucleic Acids Res*. 2015;43:10588-10601. doi 10.1093/nar/gkv1166

Maréchal A., Zou L. DNA damage sensing by the ATM and ATR kinases. *Cold Spring Harbor Perspect Biol*. 2013;5(9):a012716. doi 10.1101/cshperspect.a012716

Meltser V., Ben-Yehoyada M., Shaul Y. c-Abl tyrosine kinase in the DNA damage response: cell death and more. *Cell Death Differ*. 2011;18(1):2-4. doi 10.1038/cdd.2010.132

Olcina M.M., Grand R.J.A., Hammond E.M. ATM activation in hypoxia – causes and consequences. *Mol Cell Oncol*. 2014;1(1):e29903. doi 10.4161/mco.29903

Pinkel D., Landegent J., Collins C., Fuscoe J., Segraves R., Lucas J., Gray J. Fluorescence in situ hybridization with human chromosome-specific libraries: detection of trisomy 21 and translocations of chromosome 4. *Proc Natl Acad Sci USA*. 1988;85(23):9138-9142. doi 10.1073/pnas.85.23.9138

Sørensen C.S., Syljuåsen R.G., Falck J., Schroeder T., Rönnstrand L., Khanna K.K., Zhou B.B., Bartek J., Lukas J. Chk1 regulates the S phase checkpoint by coupling the physiological turnover and ionizing radiation-induced accelerated proteolysis of Cdc25A. *Cancer Cell*. 2003;3:247-258. doi 10.1016/S1535-6108(03)00048-5

Stefler D., Malyutina S., Maximov V., Orlov P., Ivanoschuk D., Nikitin Y., Gafarov V., Ryabikov A., Voevoda M., Bobak M., Holmes M.V. Leukocyte telomere length and risk of coronary heart disease and stroke mortality: prospective evidence from a Russian cohort. *Sci Rep*. 2018;8(1):16627. doi 10.1038/S41598-018-35122-y